RESEARCH ARTICLE

Key Points:
- Water levels from two wells in Israel show sustained change induced by teleseismic waves
- Pressure oscillations and sustained changes are modeled using the continuum damage-porosity model
- Compaction and damage control the sustained water-level increase/decrease, respectively

Correspondence to:
E. Shalev,
eyal@gsi.gov.il

Sustained water-level changes caused by damage and compaction induced by teleseismic earthquakes

Eyal Shalev[1], Ittai Kurzon[1], Mai-Linh Doan[2], and Vladimir Lyakhovsky[1]

[1]Geological Survey of Israel, Jerusalem, Israel, [2]Institut des Sciences de la Terre (ISTerre), Université Grenoble-Alpes, Saint-Martin-d'Hères, France

Abstract Sustained water-level increase and decrease induced by distant earthquakes were observed in two wells, Gomè 1 and Meizar 1 in Israel. The Gomè 1 well is located within a damage zone of a major fault zone, and Meizar 1 is relatively far from a fault. The monitored pressure change in both wells shows significant water-level oscillations and sustained water-level changes in response to the passage of the seismic waves. The sustained water-level changes include short-term (minutes) undrained behavior and longer-period (hours and days) drained behavior associated with groundwater flow. We model the short-term undrained response of water pressure oscillations and sustained change to the distant 2013 M_w 7.7 Balochistan earthquake by nonlinear elastic behavior of damaged rocks, accounting for small wave-induced compaction and damage accumulation. We suggest that the rocks are close to failure in both locations and strain oscillations produced by the passing seismic waves periodically push the rock above the yield cap, creating compaction when volumetric strain increases and damage when shear strain increases. Compaction increases pore pressure, whereas damage accumulation decreases pore pressure by fracture dilation. The dominant process depends on the properties of the rock. For highly damaged rocks, dilatancy is dominant and a sustained pressure decrease is expected. For low-damage rocks, compaction is the dominant process creating sustained water-level increase. We calculate damage and porosity changes associated to the Balochistan earthquake in both wells and quantify damage accumulation and compaction during the passage of the seismic waves.

1. Introduction

Dynamic triggering of earthquakes by seismic waves is well documented, but the mechanisms by which dynamic triggering occurs are currently unknown [*Brodsky and van der Elst*, 2014]. Most of the macroscopic observations related to distant earthquakes are hydrological and relate to permeability enhancement [*Manga et al.*, 2012; *Xue et al.*, 2013]. Seismic waves are known to cause oscillations in well water levels and in some occasions also to cause sustained water-level changes [*Ben-Zion et al.*, 1990; *Brodsky et al.*, 2003; *Crews and Cooper*, 2014; *Doan and Cornet*, 2007; *Manga et al.*, 2012; *Roeloffs et al.*, 2003; *Roeloffs*, 1998; *Shi et al.*, 2015a; *Shi et al.*, 2015b; *Wang and Manga*, 2010; *Yan et al.*, 2014; *Zhang et al.*, 2015]. These observations and models account for sustained changes of the water level occurring during different periods. In some wells, the short-term sustained coseismic water-level changes always have the same sign; some wells have only water-level decrease and some only water-level increase [*Brodsky et al.*, 2003]. Different mechanisms for coseismic well water-level changes have been discussed. Among them are the intrusion of hot groundwater [*Roeloffs et al.*, 2003], unclogging of the colloidal filling of fractures [*Brodsky et al.*, 2003], mobilization of pore-clogging gas bubbles [*Roeloffs*, 1998], and gas bubble nucleation and growth [*Crews and Cooper*, 2014].

Here we associate the duration of the short-term (minutes) sustain change with the passage of the seismic waves and assume that they occur under undrained conditions. The longer-period changes (hours and days) reflect drained conditions, in which the water level in the well is affected by groundwater flow. *Shalev et al.* [2016] showed that undrained short-term water level responds dramatically to both volumetric deformation (*P* and Rayleigh waves) and deviatoric strain (*S* and Love waves). The latter is explained by the nonlinear elastic behavior of highly damaged rocks and speculated that sustained water-level changes may be a result of the small damage and porosity change of the aquifer. In this paper we present new observations of sustained water-level changes and connect them to small damage increase and porosity decrease
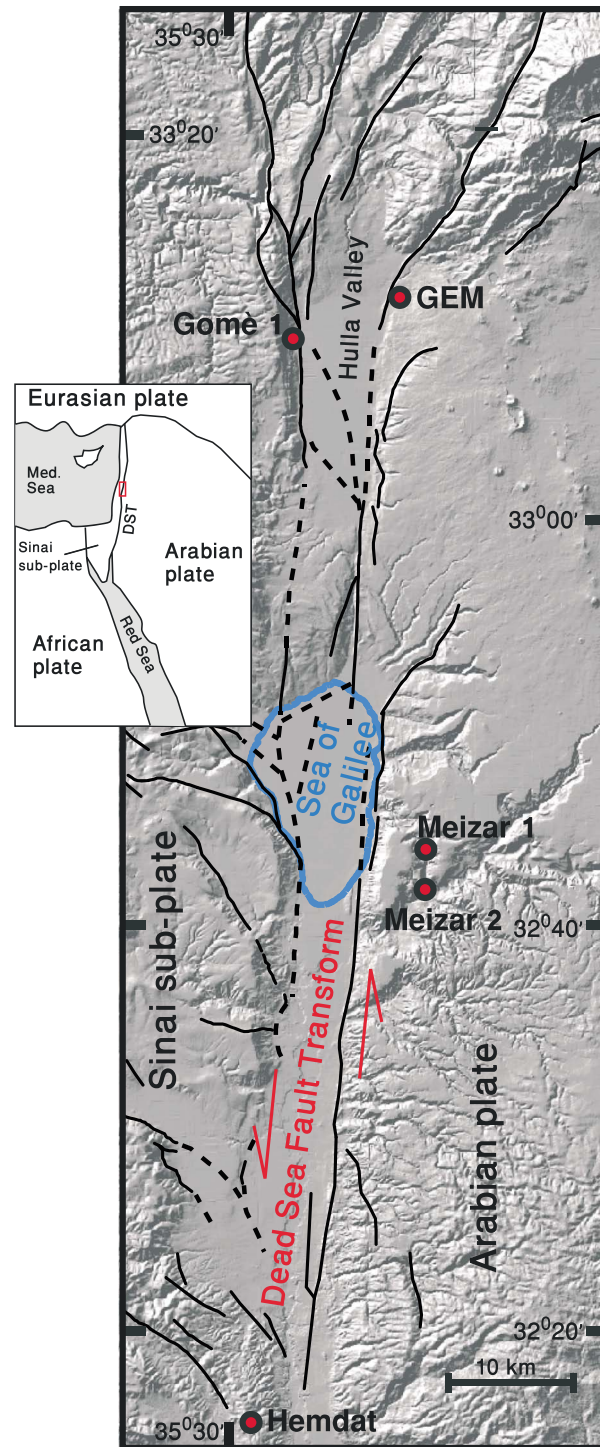
Figure 1. Map of the main faults of the northern Dead Sea Rift and locations of Gomè 1 and Meizar 1 and Givat Ha'em (GEM) seismic stations, modified after *Sneh and Weinberger* [2014].

(compaction) produced by travelling seismic waves, utilizing the continuum damage-porosity model from *Lyakhovsky et al.* [2015]. We distinguish between the effects of poroelastic (seconds) damage (minutes) and hydrological (days) on the water pressure.

2. Hydrogeological Setting

The wells Gomè 1 and Meizar 1 and 2 are located on both sides of the Dead Sea Transform (DST). The DST is an intra-continental left-lateral transform accommodating the relative motion between the African (Sinai) and Arabian plates (Figure 1). The Hula Valley is considered to be a rhomb-shaped graben, which subsided in stages during the last 4 Ma [*Weinberger*, 2014; *Weinberger et al.*, 2009]. The Gomè and Meizar wells differ in their lithology and in their proximity to deformation zones.

2.1. Gomè 1 Well

The artesian Gomè 1 well is located 80 m from a major fault that defines the western boundary of the Hula pull-apart, 33°9′4″N latitude, 35°34′10.4″E longitude (Figure 1). The 396 m deep well was drilled down to the Kurnub sandstone group that is confined by a 70 m thick clay layer. Gomè 1 is an artesian (closed) well with water overpressure of ~0.08 MPa. The deepest 100 m of the well is installed with screens against the permeable layers (~60 m) and casing against the clay layers (~40 m). Hydraulic conductivity of $K = 0.05$ m/d and specific storage of $S_s = 2.5 \times 10^{-6}$ were calculated using tidal analysis [*Shalev et al.*, 2016]. Based on the response of water pressure to deviatoric deformation, *Shalev et al.* [2016] suggested that Gomè 1 is located within highly fractured rocks.

2.2. Meizar 1 Well

The 1250 m deep well, 32°44′32″N latitude, 35°41′46″E longitude (Figure 1), was drilled down to the Judea dolostone group that is confined by a 900 m thick clay, chalk, and chert layers of Mount Scopus Group. The deepest 200 m of the well opens against the highly permeable dolostone layers. Meizar 1 well is relatively far from a fault (~5.5 km). It is an open well with water level about 100 m below the surface.
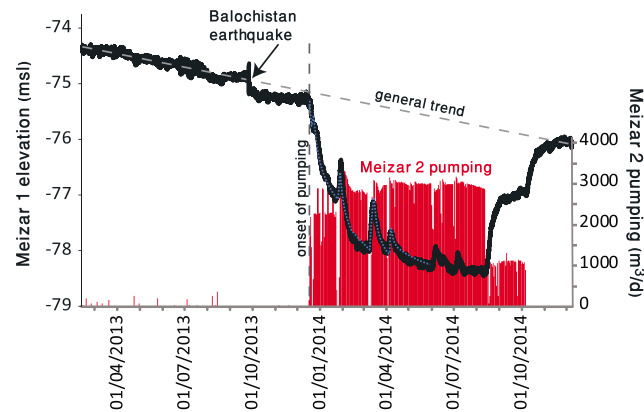
Figure 2. Water levels at Meizar 1 along with pumping at Meizar 2. The response of the water levels at Meizar 1 is modeled using AQTESOLV to fit pumping at Meizar 2 (blue dashed line). The general trend of the water levels reflects the aquifer overexploitation.

2.3. Meizar 2 Well

The 807 m deep well located 3 km south of Meizar 1 (Figure 1) was also drilled down to the Judea dolostone group. Its elevation is 150 m lower than Meizar 1, and therefore, the water pressure is artesian. The deepest 220 m of the well opens against the highly permeable dolostone layers. However, Meizar 2 is often pumped and therefore does not have a continuous monitoring. Hydraulic conductivity and specific storage were calculated using AQTESOLV [*Duffield*, 2007] based on the response of the water level at Meizar 1 to pumping at Meizar 2 (Figure 2). Water levels at Meizar 1 are modeled to respond to every pumping rate at Meizar 2 (blue dashed line at Figure 2) with hydraulic conductivity of $K = 2$ m/d and specific storage of $S_s = 7.5 \times 10^{-7}$. Tidal analysis reported by *Shalev et al.* [2016] yield similar values. The general trend of the water levels reflects aquifer overexploitation.

The hydraulic parameters for both wells did not change during the monitoring period, and there was no evidence for recognized seismically induced transmissivity change.

3. Hydroseismic Data

Seismic data were obtained from the Geophysical Institute of Israel network station, Givat Ha'em (GEM), 11 km northeast of Gomè 1, and Hemdat (HMDT), 55 km south-southwest of Meizar 1 and 2 (see Figure 1 for location). GEM is a broadband seismic station, with a third-generation STS-2 sensor (Streckeisen), and a Europe Trident digitizer (Nanometrics), set to a 40 V peak to peak sensitivity and to a sampling frequency of 40 Hz. HMDT is a broadband seismic station, with a Trillium Compact 120 sensor (Nanometrics), and a Trident digitizer (Nanometrics), set to a 40 V peak to peak sensitivity and to a sampling frequency of 40 Hz.

Coseismic water-level changes in both wells were recorded for several distant earthquakes and local events along the Dead Sea Transform. The strong intermediate distant earthquake Balochistan, Pakistan (24 September 2013 $M_w = 7.7$) shows the most clear waveforms and coseismic water-level oscillations observed in both Gomè 1 and Meizar 1, ~3000 km ($\Delta = 26.5°$) away from the epicenter (Figure 3). This Balochistan earthquake ruptured 200 km of the Hoshab Fault in Pakistan with large inelastic shortening and produced the second-largest lateral surface displacement observed for a continental strike-slip earthquake [e.g., *Gold et al.*, 2015; *Vallage et al.*, 2015]. The drained response of water levels in both wells to the earthquake includes continuous decrease for a few days (Figures 3a and 3b). We speculate that this response reflects permeability enhancement of nearby faults that create shortcuts between aquifers. The high groundwater overpressure at Gomè 1 is suggested to be released through the fault, which is only tens of meters away. At Meizar 1, the pressure of the groundwater is also high, but it is about 5 km away from a major fault. However, as evident from the response of the water level to pumping at Meizar 2, such a distance is considered to be within the response radius of pumping. The response of the water level to the largest aftershock ($M_w = 6.8$) of the Balochistan earthquake and to the $M_w = 6.4$ Crete earthquake are also recognized in Gomè 1 (Figure 3a). The undrained short-term response of water levels is different for the two wells; at Gomè 1 water pressure decreases (Figures 3c and 3e), whereas at Meizar 1 water pressure increases (Figures 3d and 3f). Similar behavior in both wells occurred in response to the 16 April 2013 M_w 7.8 Saravan earthquake in Iran ~2600 km ($\Delta = 23.2°$) away from the epicenter (Figure 4). We propose that these observations are related to damage accumulation and compaction.

GEM and HMDT stations recorded the seismic waves generated by the Balochistan earthquake (Figure 5). *Shalev et al.* [2016] calculated strain components from the seismograms and correlated them to the
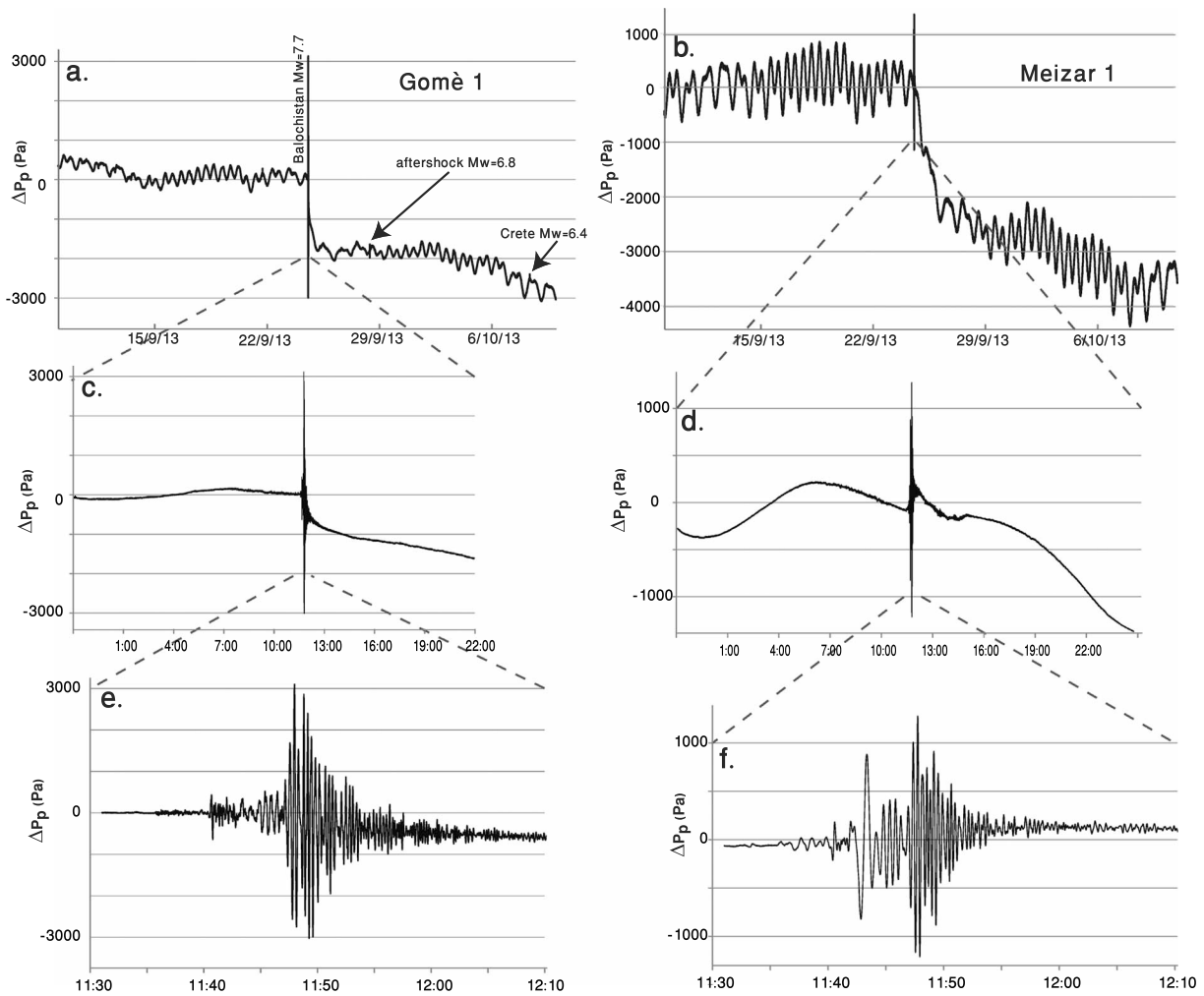
Figure 3. Water-level responses at Gomè 1 and Meizar 1 to the 24 September 2013 M_w 7.7 Balochistan earthquake. (a) Drained response in Gomè 1, (b) drained response in Meizar 1, (c) undrained response in Gomè 1, (d) undrained response in Meizar 1, (e) undrained hydroseismogram response in Gomè 1, and (f) undrained hydroseismogram response in Meizar 1.

detrended water-level oscillation and undrained sustain changes in both wells ignoring sustained change. In this study, we use their strain-water pressure correlation to calculate damage accumulation and compaction and estimate their effects on the undrained sustain water change.

The seismic records (seismograms) from the relatively close earthquakes such as the 12 October 2013 $M_w = 6.4$ Crete, $\Delta = 10.396°$ (Figure 6a), and 24 May 2014 $M_w = 6.9$ Aegean Sea, $\Delta = 10.822°$, as well as local events, do not show a good separation between the Love and Rayleigh phases; the recorded waveforms do not allow calculating correctly the coseismic strain components associated with velocity and direction
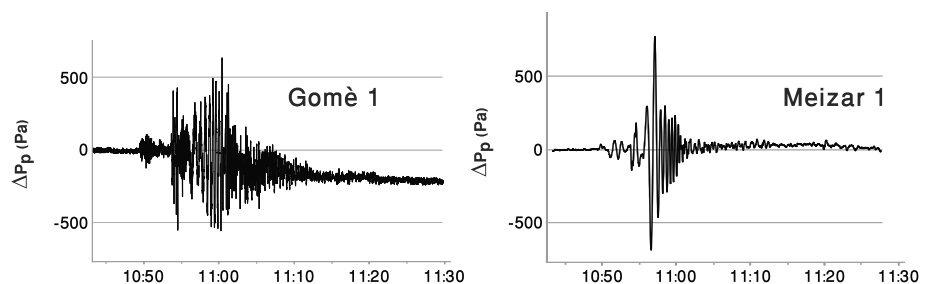

Figure 4. Water-level responses at Gomè 1 and Meizar 1 to the 16 April 2013 M_w 7.8 Saravan earthquake.
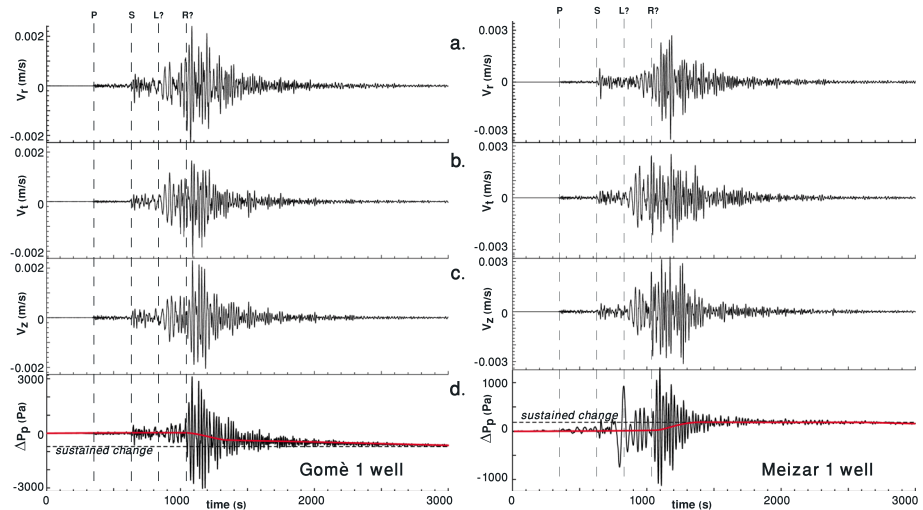
Figure 5. Seismograms and water-level responses to the 24 September 2013 M_w 7.7 Balochistan earthquake. (a) Radial, (b) transversal, and (c) vertical components of seismograms and (d) water-level changes recorded at Gomè 1 and Meizar 1. Sustained water-level increase (200 Pa) is observed in Meizar 1 and decrease (700 Pa) in Gomè 1.

of each phase. On the other hand, for the relatively distant earthquakes, such as the 24 May 2013 $M_w = 8.3$ Sea of Okhotsk, $\Delta = 77.011°$ (Figure 6b), or 25 April 2015 Nepal $M_w = 7.8$, $\Delta = 42.1°$, the amplitudes of the coseismic water-level changes are very small and the expected sustained water-level changes are below the instrumental resolution.

4. Strain-Pore Pressure Coupling

The amplitude of water-level oscillations in a well in response to seismic waves depends on the characteristics of seismic waves, aquifer properties, and geometrical dimensions of the well [*Cooper et al.*, 1965]. *Skempton* [1954] formulated a poroelastic law in which deviatoric stress changes might also affect pore pressure:

$$\Delta p_f = -B\left[\Delta\sigma_m + 2\left(A - \frac{1}{3}\right)\Delta\sigma_d\right] \tag{1}$$
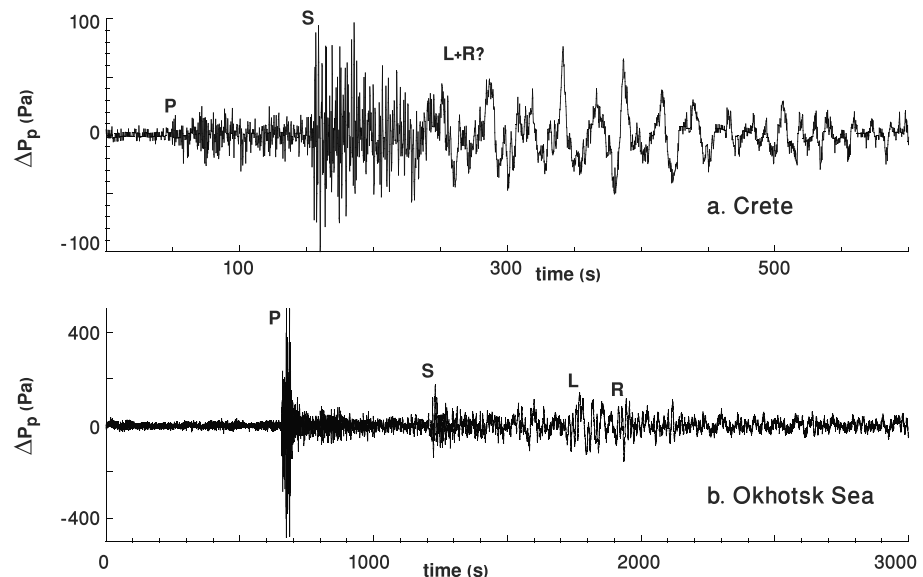

Figure 6. Water-level responses at Gomè 1 to (a) $M_w = 6.4$ Crete earthquake and (b) $M_w = 8.3$ Sea of Okhotsk earthquake.
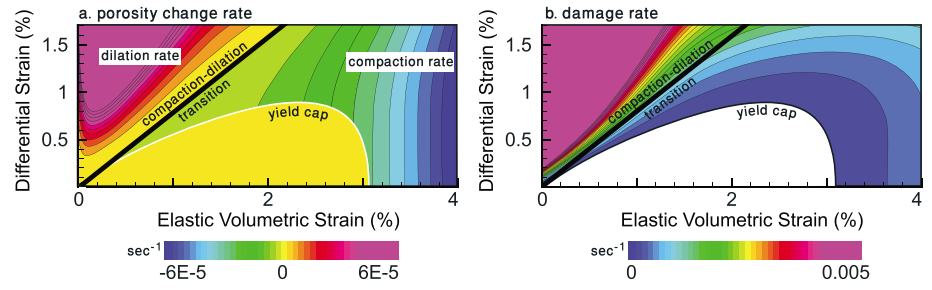
Figure 7. Rates of (a) porosity and (b) damage changes as a function of differential and volumetric strains for sandstone. Below the yield cap, there is no damage accumulation.

where A and B are the Skempton coefficients, $\sigma_m = \frac{1}{3}(\sigma_1 + \sigma_2 + \sigma_3)$ is the mean stress, and $\sigma_d = \frac{\sigma_1 - \sigma_3}{2}$ is the deviatoric stress for uniaxial loading ($\sigma_2 = \sigma_3$). *Henkel and Wade* [1966] and *Holtz and Kovacs* [1981] generalized equation (1) to a three-dimensional state of stress, but the case of arrival of seismic waves from relatively distant earthquake is simplified to a two-dimensional problem.

Because seismic data are collected by recording ground velocity, *Shalev et al.* [2016] rewrote equation (1) in terms of strain:

$$\Delta p_f = \Delta \left[BK_u \left(\varepsilon_v + \frac{\zeta - \phi}{\alpha_B} \right) + N\varepsilon_d \right] \tag{2}$$

where K_u is the undrained bulk modulus [*Wang*, 2000], ε_v is the volumetric strain, ϕ is the porosity, ζ is the water content, α_B is the Biot coefficient, $N = -4\mu B\left(A - \frac{1}{3}\right)$ is the shear strain coupling coefficient, μ is the shear modulus, and $\varepsilon_d = \frac{\varepsilon_1 - \varepsilon_3}{2}$ is the deviatoric strain. For a linear poroelastic material with no volumetric-shear coupling, $A = 1/3$ and $N = 0$. Rocks under shear loading develop fractures and dilate. *Lyakhovsky et al.* [2015] in their model formulation assumed that the Skempton coefficient B multiplied by the undrained bulk modulus K_u is preserved unchanged during damage accumulation ($BK_u = \text{const}$). *Shalev et al.* [2016] presented the functional relation $N(\alpha_D)$ (their equation (3) and Figure 7) between the coupling coefficient and the damage parameter changing within the range of $0 < \alpha_D < 1$. They showed that $N = 0$ for intact damage-free rock ($\alpha_D = 0$) and can be even larger than BK_u with damage approaching $\alpha_D = 1$ for completely destroyed rock. As damage accumulates, the coupling between volumetric and shear strain increases. Assuming that the tectonic strain (volumetric ε_v and deviatoric ε_d) and the water content ζ before and after the passage of the seismic waves remain the same, the short-term undrained sustained pore pressure change Δp_f^s is defined as the average change induced by the porosity and damage variations:

$$\Delta p_f^s = -\frac{BK_u}{\alpha_B} \Delta\phi + \frac{\partial N}{\partial \alpha_D} \Delta\alpha_D \varepsilon_d \tag{3}$$

Equation (3) is used here for calculating the sustain water pressure changes (the difference between after and before teleseismic earthquake), whereas equation (2) is used for water pressure oscillation during the passage of the seismic waves.

5. Porosity and Damage Changes During Oscillations

During the passage of seismic waves, rocks are periodically subjected to volumetric and shear strain changes. We model the pressure oscillations and sustained changes using the continuum damage-porosity model presented by *Lyakhovsky et al.* [2015], which considers two thermodynamic state variables: porosity and damage intensity, coupled by kinetic relations. The model predicts that the volumetric and shear strains have the potential to cause damage and shear-enhanced (damage-induced) compaction that could lead to sustained water-level changes. Rock compaction and damage increase cause opposite signs of the water pressure change. Compaction leads to sustained water-level increase, whereas accumulated damage leads to enhanced dilatancy and sustained water-level decrease. Competition between these two processes may explain different sustained water-level changes in different wells. The dominating processes (compaction or damage accumulation) depend on the stress (or strain) regime and on the properties of the rock.

The model suggested by *Lyakhovsky et al.* [2015] addresses three different deformation regimes that are defined by two envelopes (Figure 7). White line defines the yield cap, and black line stands for the transition between compaction and dilation. These lines define three zones in the differential-volumetric strain diagram. Beneath the yield cap the elastic deformation is characterized by relatively high volumetric and low shear strain components. At geological time scales, these loading conditions may cause slow material strengthening associated with crack closure and compaction (porosity decrease). However, this process is negligible for the time scales of the present study associated with wave-induced effects. Therefore, rates of compaction and damage changes are not included in this model when strains are below the yield cap (Figure 7). With relatively high shear and low volumetric strain, beyond the compaction-dilation transition, intensive damage accumulation along with significant differential strains lead to material dilation (porosity increase). Transition to this unstable regime associated with macroscopic failure will lead to dynamic triggering of earthquakes [*Rice et al.*, 2014]. The sustained water-level changes are associated with intermediate shear and volumetric strain, between the yield cap and the compaction-dilation transition. In this regime, the model assumes that damage increase and porosity decrease have opposite effects on the fluid pressure changes.

The accumulated damage and porosity changes are a result of the integrated rates over time during the oscillating loads. The rates of porosity (Figure 7a) and damage (Figure 7b) changes are defined by two coupled kinetic equations, which are slightly different for different deformational regimes (see *Lyakhovsky et al.* [2015] for detailed discussion).

Above the yield cap the rate of damage accumulation is [*Lyakhovsky et al.*, 2015]

$$\frac{d\alpha_D}{dt} = C_d \left[D(\zeta)(-I_1)^{n+1} + I_2(\xi - \xi_0) \right] \tag{4}$$

where C_d is the kinetic coefficient of the damage accumulation and $I_1 = \varepsilon_{kk}$ and $I_2 = \varepsilon_{ij}\varepsilon_{ij}$ are the first and second invariants of the strain tensor. The power index $n > 1$, the strain invariant ratio $\xi = I_1/\sqrt{I_2}$, the critical strain invariant ratio ξ_0, and the function $D(\zeta)$ of the water content define the shape of the yield cap or the onset of the damage accumulation.

The damage accumulation above the yield cap causes shear-enhanced or damage-induced compaction at values of strain invariant ratio below critical ($\xi < \xi_0$). At higher shear strains (high ξ values), the model predicts the damage-induced dilation. This behavior is described by the kinetic equation for the porosity change [*Lyakhovsky et al.*, 2015]:

$$\frac{d\phi}{dt} = C_d D(\zeta)(-I_1)^n \frac{\gamma_r}{K_u} I_2(\xi - \xi_0) \tag{5}$$

where γ_r is the strain coupling modulus for completely destroyed material ($\alpha_D = 1$). The sign of the term ($\xi - \xi_0$) on the right-hand side of equation (5) defines the mode of the porosity evolution, i.e., compaction ($d\phi/dt < 0$) or dilation ($d\phi/dt > 0$). Thus, the condition $\xi = \xi_0$ defines the compaction-dilation transition shown in Figure 7. Calibrated model parameters against laboratory experiments with Berea sandstone are presented by *Lyakhovsky et al.* [2015].

Both processes (compaction and damage changes) affect the volumetric strain and the pore pressure (equation (3)). Changes in porosity directly change pore pressure, and changes in damage state change the coupling between shear and volumetric strains. Using the two terms of equation (3) and the parameters of *Lyakhovsky et al.* [2015], it is possible to quantify the rate of the pore pressure change (Figure 8). Whether the rate of fluid pressure is positive or negative depends on the role of the controlling mechanism (compaction or damage accumulation) at a given strain state. Since the damage-induced pressure change (equation (3)) depends on the value of $\frac{\partial N}{\partial \alpha_D}$, which differs by orders of magnitude between low- and high-damage rocks [*Shalev et al.*, 2016], the expected pore pressure changes at low-damage (Figure 8a) and high-damage (Figure 8b) values are different. Slightly above the yielding (location marked by star in zoomed Figure 8), compaction dominates the pressure increase at low-damage values, whereas damage dominates pressure decrease at high-damage values. At low-damage state, there is a large strain range in which there is a positive pore pressure change and the rock will experience sustained pore pressure increase (Figure 8a). At high-damage state, for the same strain state, there is a negative pore pressure change and the rock will experience sustained pore pressure decrease (Figure 8b). Using the mapped rates of pore pressure changes, the overall
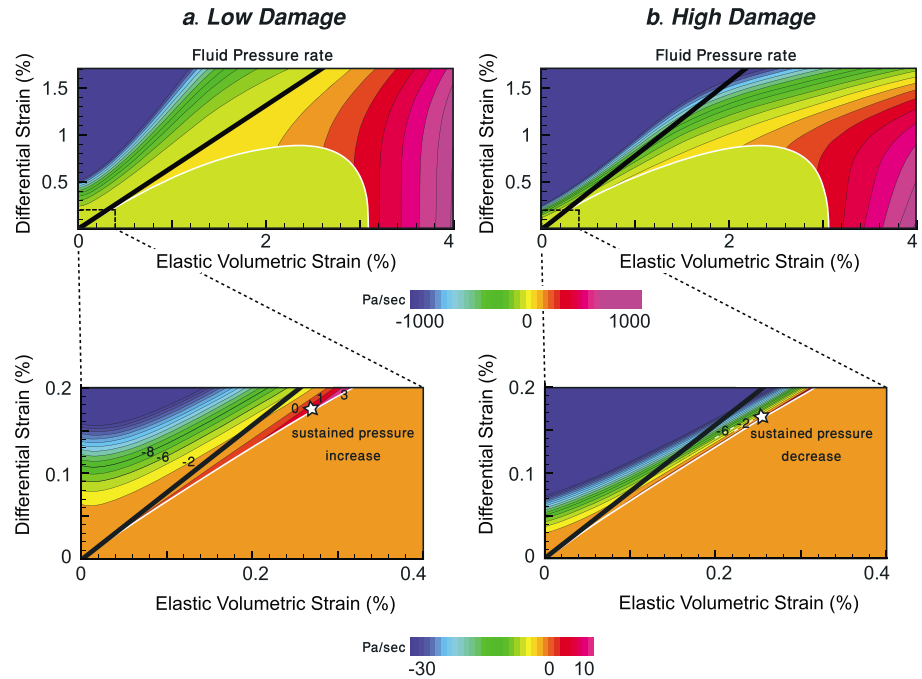
Figure 8. Pore pressure rate of change of a rock with (a) low damage and (b) high damage. The stars represent a strain state in which there is a pore pressure increase for a rock with low damage and a decrease for a rock with high damage.

amount of sustained pressure change can be calculated by integrating the strain-dependent rate of the pressure change over the time that the rock spends at a given strain state.

6. Data Processing

Meizar 1 is an open well, and therefore, high-frequency water-level oscillations are attenuated. Meizar 2 is a closed well located 3 km south of Meizar 1 and open to the same aquifer. Unfortunately, water level at Meizar 2 was not monitored during the Balochistan earthquake. However, other earthquakes induced water-level oscillations that were monitored in both Meizar 1 and 2. The records show that the oscillations in Meizar 1 are attenuated by a factor of 12 with respect to the oscillations in Meizar 2 (Figure 9). Therefore, in our calculations, the amplitude of the oscillations is multiplied by 12.

The three velocity channels (E, N, and Z) of the seismic waveforms and the fluid pressure were segmented and aligned by the origin time of the event. The three velocity channels were rotated horizontally to the radial and transversal components and then picked for their P, S, Love, and Rayleigh arrivals. Calculated strains
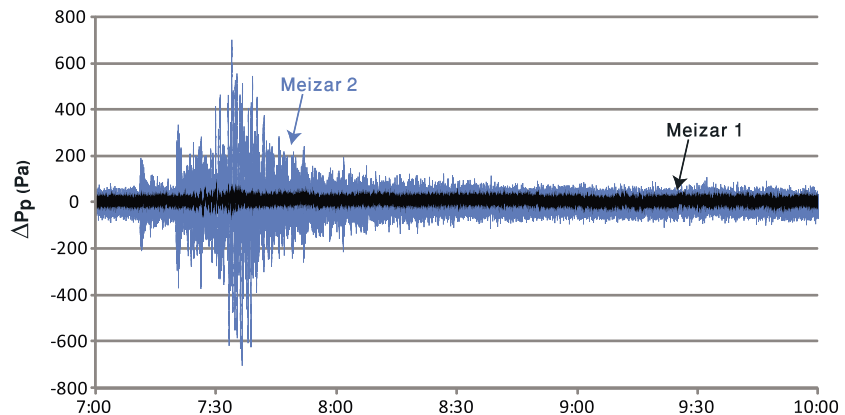

Figure 9. Water-level responses at Meizar 1 and 2 to the 12 May 2015 M_w 7.3 Nepal earthquake.
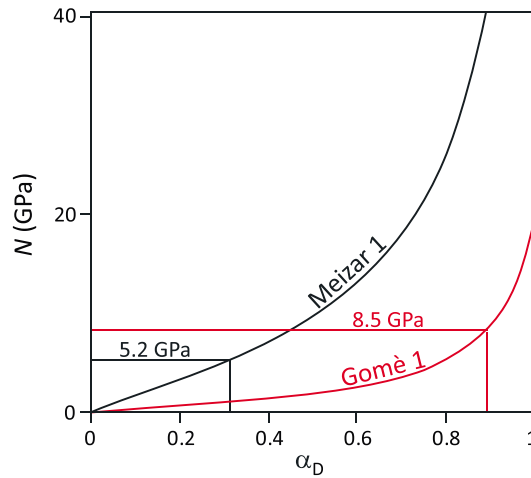
Figure 10. The deviatoric coupling terms, N, as a function of damage state. The calculated N value corresponds to $\alpha_D = 0.9$ for Gomè 1 and $\alpha_D = 0.3$ for Meizar 1.

and measured fluid pressure were demeaned and smoothed using high-pass Butterworth filter with a bottom corner frequency of 0.001 Hz and 4 p [*Shalev et al.*, 2016]. In addition, the velocity waveforms and the fluid pressure were downsampled to 1 Hz. The obtained signals were used for cross-correlation procedure reported by *Shalev et al.* [2016] for Gomè 1 and extended here for Meizar 1. Their results exhibit high correlation, resulting with well-constrained values of $BK_u = 11.4$ GPa, $N = 8.5$ GPa for Gomè 1. The same procedure for Meizar 1 gives $BK_u = 35.6$ GPa, $N = 5.2$ GPa. The obtained BK_u values are compatible with published values for sandstone (Gomè 1) and dolostone (Meizar 1).

7. Water Pressure Changes in Gomè 1 and Meizar 1

The change of the shear strain coupling coefficient, N, with damage was formulated by *Shalev et al.* [2016]. N versus α_D is calculated, assuming that stress is close to the yield envelope, $\xi = \xi_0$ for two different BK_u values corresponding to Gomè 1 and Meizar 1 (Figure 10). The values obtained by the coupled strain-pore pressure modeling corresponds to a damage values of $\alpha_D = 0.9$ for Gomè 1 ($N = 8.5$ GPa) and $\alpha_D = 0.3$ for Meizar 1 ($N = 5.2$ GPa). Using N versus α_D (Figure 10), it is now also possible to numerically differentiate N with respect to α_D. The term $\frac{\partial N}{\partial \alpha_D}$ that controls the sustained pore pressure change (equation (3)) also depends on damage (Figure 11). At Gomè 1 $\frac{\partial N}{\partial \alpha_D}$ is 50 GPa, and at Meizar 1 it is 20 GPa.

We estimated the volumetric strain component associated with the depth of each well (Gomè 1: 400 m and Meizar 1: 1200 m) and assumed that the rocks are critically stressed [*Zoback et al.*, 2002]. Since the Balochistan earthquake caused significant strain oscillations at Gomè 1 and Meizar 1, manifested by water pressure oscillation and sustained changes, we locate the tectonic strain to be close to the yielding cap (marked as a star in Figure 12). Oscillations associated with seismic waves move the state of strain periodically around its initial location, corresponding to the tectonic load. For the estimated tectonic strain, the wave-induced oscillations shift the strain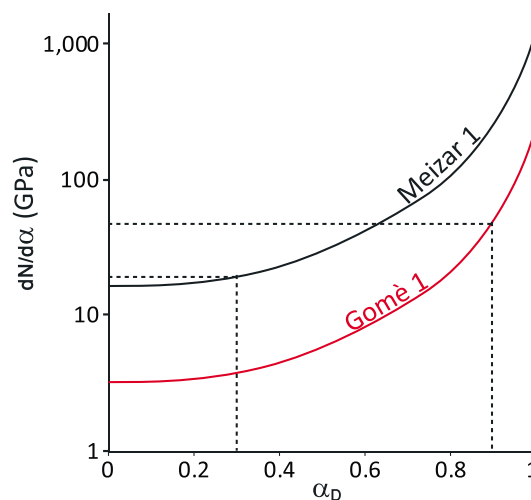 above the yield cap in both wells. Black dots in Figure 12 demonstrate the peak strains during the passage of seismic waves. Some of the peak strains are elevated above the yield cap, meaning that compaction and damage accumulation occur during short duration within each seismic oscillation. In Gomè 1, located in highly damaged rocks, strain oscillations caused mainly negative pore pressure changes (Figure 12a), whereas in Meizar 1, located in low-damage rocks, they caused mainly positive pore pressure changes (Figure 12b). The integrated amount of compaction and damage accumulation together with wave-induced pressure change is shown in
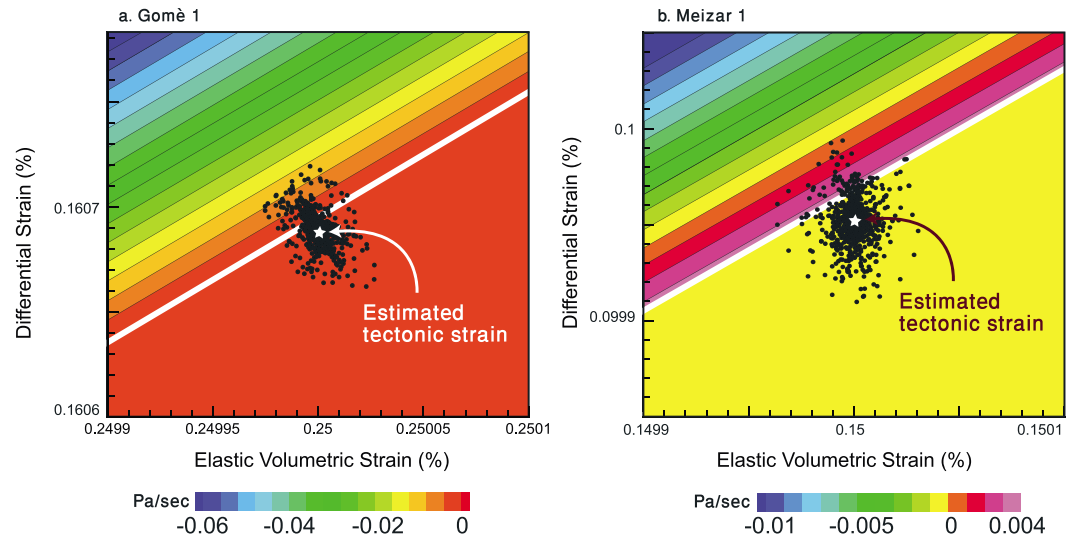

Figure 11. The term $\frac{\partial N}{\partial \alpha_D}$ that controls the sustained water-level changes (equation (3)) as a function of α_D. At Gomè 1 $\frac{\partial N}{\partial \alpha_D}$ is 50 GPa, and at Meizar 1 it is 20 GPa.

Figure 12. Pore pressure rate of change at Gomè 1 and Meizar 1. Black dots represent the peaks of strain oscillations associated with the distant Balochistan earthquake.

Figure 13 for both Gomè 1 and Meizar 1. Step-like shape of the curves for porosity and damage change shows that the rock properties are changed during relatively short duration within each seismic oscillation when the strain is above the yield cap. In Gomè 1 damage accumulation is 5 times higher than compaction, and in Meizar 1 compaction is 4 times higher than damage accumulation. This difference is obtained using the same parameters in the kinetic equations (equations (4) and (5)) and is associated with different depth of each well. The calculated pressure change fits well both oscillations and sustained pressure components measured in Gomè 1 and Meizar 1 wells (Figure 13).

8. Discussion

The distant Saravan (Figure 4) and Balochistan (Figure 5) earthquakes caused significant strain oscillations at Gomè 1 and Meizar 1 that were manifested by water pressure oscillations and sustained changes. These oscillations are more than 10 times larger than oscillations induced by the earthquakes that did not induced sustained water-level changes (Figure 6). We suggest that in both locations the tectonic stress is close to yield and wave-induced oscillations periodically move the state of stress above the yield cap and cause irreversible compaction and damage accumulation. We utilize the continuum damage-porosity model to calculate the effect that each process, compaction and damage accumulation, has on the water-level change and compare it with the observed levels in two wells. Although damage and porosity changes induced by teleseismic oscillations are small (Figure 13), when multiplied by large factors on the order of 10 GPa, the resulting sustained
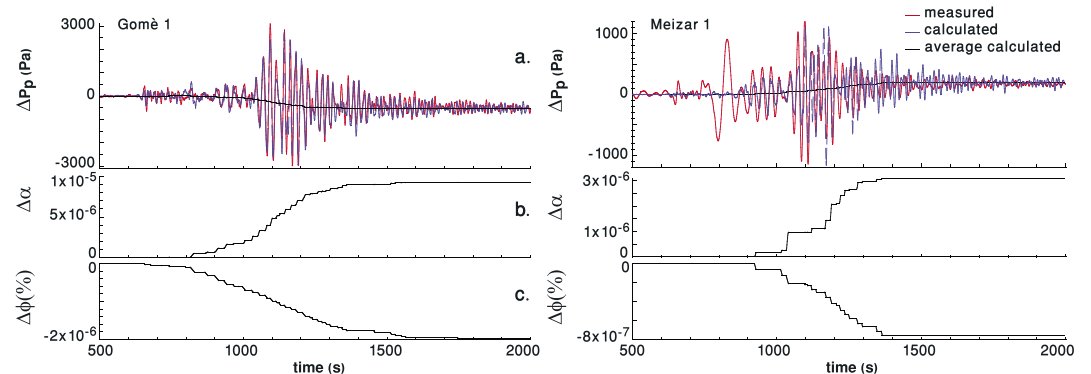

Figure 13. (a) Measured and calculated water pressure at Gomè 1 and Meizar 1. Water pressure is calculated using (b) damage accumulation and (c) porosity changes.

water pressure changes are in the order of hundreds of pascal corresponding to few centimeters of level change. For example, substituting into equation (3), the porosity change at Meizar 1 $\Delta\phi \sim 10^{-6}$ % multiplied by the $BK_u = 35.6$ GPa and $\alpha_B \sim 1$ gives a pressure increase of ~285 Pa. The damage increase of $\Delta\alpha_D \sim 3\ 10^{-6}$ multiplied by $\frac{\partial N}{\partial\alpha_D} = 20$ GPa and differential strain of 0.16% gives pressure decrease of ~90 Pa. The resulted overall pressure increase is ~200 Pa (2 cm). This emphasizes the sensitivity of water-level changes to compaction and damage changes. The hydraulic parameters, hydraulic conductivity and specific storage, could have been affected by these porosity and damage changes. However, these changes are below the sensitivity of tidal analysis and are not detected.

Laboratory [e.g., *Dieterich*, 1978; *Johnson and Jia*, 2005] and field [e.g., *Wu et al.*, 2009] data indicate the fast logarithmic healing of damage on short time scales under relatively high confining pressure or normal stress and low shear loading. These loading conditions are established following dynamic ruptures with a significant stress drop. The damage induced by teleseismic earthquakes was not high enough to trigger seismic events at Gomè 1 and Meizar 1 during the study period, and the loading conditions remain close to yielding with relatively high shear stress; therefore, no healing is expected.

The presented calculations suggest that distant earthquake can cause irreversible compaction and damage and change the mechanical properties of rocks thousands of kilometers from the earthquake origin. We speculate here that these wave-induced porosity and damage changes may trigger seismicity at greater depths. When extremely damaged rocks are loaded above the yield cap, small damage increase may lead to loss of rock mass stability and nucleation of local seismic event. Framework of the continuum damage-porosity model predicts that the amount of damage accumulated during the passage of teleseismic waves depends on their amplitude, frequency, and duration, as well as on the orientation of the local strain regime. Higher amplitudes and durations result with temporary longer strain state above the yield cap and longer durations of damage accumulation. These trends were also suggested for dynamic earthquake triggering [*Brodsky and Prejean*, 2005; *Brodsky and van der Elst*, 2014; *Gomberg et al.*, 2001; *Hill*, 2012; *Hill et al.*, 1993; *Pollitz et al.*, 2012].

9. Conclusions

Water levels from two wells in Israel show strong oscillations and short-term sustained changes caused by travelling seismic waves. The sustained water-level changes induced by the distant $M_w = 7.7$ Balochistan earthquake include short-term (minutes) undrained response and longer-period (hours and days) groundwater flow. Strain oscillations push the rocks in Gomè 1 and Meizar 1 above the yield cap and cause sustained water-level change. When strain is above the yield cap two competing processes occur: (1) porosity compaction and (2) damage accumulation (fracture dilation). The amount of compaction and damage accumulation depend on the amplitude, frequency, and duration of the strain oscillations. The rate of fracture dilation strongly depends on the damage level of the rocks. At high damage, the rock undergoes high dilation, whereas the porosity compaction will remain at the same order of magnitude. Therefore, the sustained water-level decrease in Gomè 1 is controlled by fracture dilation (decrease water level), whereas the sustained increase in Meizar 1 is controlled by compaction (increase water level). The proposed mechanism suggests rock damage increase during the passage of seismic waves that might enhance the time-dependent damage accumulation and promote delayed failure.

References

Ben-Zion, Y., T. L. Henyey, P. C. Leary, and S. P. Lund (1990), Observations and implications of water well and creepmeter anomalies in the Mojave segment of the San Andreas fault zone, *Bull. Seismol. Soc. Am.*, *80*(6A), 1661–1676.

Brodsky, E. E., and N. J. van der Elst (2014), The uses of dynamic earthquake triggering, *Annu. Rev. Earth Planet. Sci.*, *42*, 317–339.

Brodsky, E. E., and S. G. Prejean (2005), New constraints on mechanisms of remotely triggered seismicity at Long Valley caldera, *J. Geophys. Res.*, *110*, B04302, doi:10.1029/2004JB003211.

Brodsky, E. E., E. Roeloffs, D. Woodcock, I. Gall, and M. Manga (2003), A mechanism for sustained groundwater pressure changes induced by distant earthquakes, *J. Geophys. Res.*, *108*(B8), 2390, doi:10.1029/2002JB002321.

Cooper, H. H., J. D. Bredehoeft, I. S. Papadopulos, and R. R. Bennett (1965), The response of well-aquifer systems to seismic waves, *J. Geophys. Res.*, *70*(16), 3915–3926, doi:10.1029/JZ070i016p03915.

Crews, J. B., and C. A. Cooper (2014), Experimental evidence for seismically initiated gas bubble nucleation and growth in groundwater as a mechanism for coseismic borehole water level rise and remotely triggered seismicity, *J. Geophys. Res. Solid Earth*, *119*, 7079–7091, doi:10.1002/2014JB011398.

Dieterich, J. H. (1978), Time-dependent friction and the mechanics of stick-slip, *Pure Appl. Geophys.*, *116*(4), 790–806.

Doan, M. L., and F. H. Cornet (2007), Small pressure drop triggered near a fault by small teleseismic waves, *Earth Planet. Sci. Lett.*, *258*(1–2), 207–218.

Duffield, G. M. (2007), AQTESOLV for Windows version 4.5 user's guide HydroSOLVE, Reston, Va.

Gold, R. D., N. G. Reitman, R. W. Briggs, W. D. Barnhart, G. P. Hayes, and E. Wilson (2015), On- and off-fault deformation associated with the September 2013 M_w 7.7 Balochistan earthquake: Implications for geologic slip rate measurements, *Tectonophysics*, *660*, 65–78.

Gomberg, J., P. Reasenberg, P. Bodin, and R. Harris (2001), Earthquake triggering by seismic waves following the Landers and Hector Mine earthquakes, *Nature*, *411*(6836), 462–466.

Henkel, D. J., and N. H. Wade (1966), Plane strain tests on a saturated remoulded clay, *J. Soil Mech. Found. Div. Am. Soc. Civ. Eng.*, *92*(SM6), 67–80.

Hill, D. P. (2012), Dynamic stresses, Coulomb failure, and remote triggering—Corrected, *Bull. Seismol. Soc. Am.*, *102*(6), 2313–2336.

Hill, D. P., et al. (1993), Seismicity remotely triggered by the magnitude 7.3 Landers, California, earthquake, *Science*, *260*(5114), 1617–1623.

Holtz, R. D., and W. D. Kovacs (1981), *An Introduction to Geotechnical Engineering*, vol. 14, pp. 733, Prentice-Hall, Englewood Cliffs, N. J.

Johnson, P. A., and X. Jia (2005), Nonlinear dynamics, granular media and dynamic earthquake triggering, *Nature*, *437*(7060), 871–874.

Lyakhovsky, V., W. Zhu, and E. Shalev (2015), Visco-poroelastic damage model for brittle-ductile failure of porous rocks, *J. Geophys. Res. Solid Earth*, *120*, 2179–2199, doi:10.1002/2014JB011805.

Manga, M., I. Beresnev, E. E. Brodsky, J. E. Elkhoury, D. Elsworth, S. E. Ingebritsen, D. C. Mays, and C.-Y. Wang (2012), Changes in permeability caused by transient stresses: Field observations, experiments, and mechanisms, *Rev. Geophys.*, *50*, RG2004, doi:10.1029/2011RG000382.

Pollitz, F. F., R. S. Stein, V. Sevilgen, and R. Burgmann (2012), The 11 April 2012 East Indian Ocean earthquake triggered large aftershocks worldwide, *Nature*, *490*(7419), 250–253.

Rice, J. R., J. W. Rudnicki, and J. D. Platt (2014), Stability and localization of rapid shear in fluid-saturated fault gouge: 1. Linearized stability analysis, *J. Geophys. Res. Solid Earth*, *119*, 4311–4333, doi:10.1002/2013JB010710.

Roeloffs, E. A. (1998), Persistent water level changes in a well near Parkfield, California, due to local and distant earthquakes, *J. Geophys. Res.*, *103*(B1), 869–889, doi:10.1029/97JB02335.

Roeloffs, E., M. Sneed, D. L. Galloway, M. L. Sorey, C. D. Farrar, J. F. Howle, and J. Hughes (2003), Water-level changes induced by local and distant earthquakes at Long Valley caldera, California, *J. Volcanol. Geotherm. Res.*, *127*(3–4), 269–303.

Shalev, E., I. Kurzon, M.-L. Doan, and V. Lyakhovsky (2016), Water-level oscillations caused by volumetric and deviatoric dynamic strains, *Geophys. J. Int.*, *204*(2), 841–851.

Shi, Z., G. Wang, M. Manga, and C.-Y. Wang (2015a), Mechanism of co-seismic water level change following four great earthquakes—Insights from co-seismic responses throughout the Chinese mainland, *Earth Planet. Sci. Lett.*, *430*, 66–74.

Shi, Z., G. Wang, M. Manga, and C. Y. Wang (2015b), Continental-scale water-level response to a large earthquake, *Geofluids*, *15*(1-2), 310–320.

Skempton, A. W. (1954), The pore-pressure coefficients A and B, *Geotechnique*, *4*(4), 143–147.

Sneh, A., and R. Weinberger (2014), Major structures of Israel and environs, in *Including a Digital Shaded Relief Map*, edited by J. K. Hall scale 1:500,000, Geol. Surv. Isr, Jerusalem.

Vallage, A., Y. Klinger, R. Grandin, H. S. Bhat, and M. Pierrot-Deseilligny (2015), Inelastic surface deformation during the 2013 M_w 7.7 Balochistan, Pakistan, earthquake, *Geology*, *43*(12), 1079–1082, doi:10.1130/G37290.1.

Wang, C.-Y., and M. Manga (2010), *Earthquakes and Water*, vol. 10, pp. 225, Springer, Heidelberg, New York.

Wang, H. F. (2000), *Theory of Linear Poroelasticity with Applications to Geomechanics and Hydrogeology*, Princeton Univ. Press, Princeton, N. J.

Weinberger, R. (2014), Pleistocene strain partitioning during transpression along the Dead Sea Transform, Metulla Saddle, northern Israel, in *Dead Sea Transform Fault System: Reviews*, edited by Z. Garfunkel, Zvi Ben-Avraham, and Elisa Kagan, pp. 151–182, Springer, Netherlands.

Weinberger, R., M. R. Gross, and A. Sneh (2009), Evolving deformation along a transform plate boundary: Example from the Dead Sea Fault in northern Israel, *Tectonics*, *28*, TC5005, doi:10.1029/2008TC002316.

Wu, C., Z. Peng, and Y. Ben-Zion (2009), Non-linearity and temporal changes of fault zone site response associated with strong ground motion, *Geophys. J. Int.*, *176*(1), 265–278.

Xue, L., et al. (2013), Continuous permeability measurements record healing inside the Wenchuan earthquake fault zone, *Science*, *340*(6140), 1555–1559.

Yan, R., H. Woith, and R. Wang (2014), Groundwater level changes induced by the 2011 Tohoku earthquake in China mainland, *Geophys. J. Int.*, *199*(1), 533–548.

Zhang, Y., L.-Y. Fu, F. Huang, and X. Chen (2015), Coseismic water-level changes in a well induced by teleseismic waves from three large earthquakes, *Tectonophysics*, *651–652*, 232–241.

Zoback, M. D., J. Townend, and B. Grollimund (2002), Steady-state failure equilibrium and deformation of intraplate lithosphere, *Int. Geol. Rev.*, *44*(5), 383–401.